Journal of Luminescence 143 (2013) 304–313

Contents lists available at SciVerse ScienceDirect

Journal of Luminescence

journal homepage: www.elsevier.com/locate/jlumin

Impurity-related linear and nonlinear optical response in quantum-well wires with triangular cross section

C.A. Duque [a,(*)], M.E. Mora-Ramos [a,b], E. Kasapoglu [c], F. Ungan [c], U. Yesilgul [c], S. Sakiroglu [d], H. Sari [c], I. Sökmen [d]

[a] Instituto de Física, Universidad de Antioquia, AA 1226, Medellín, Colombia
[b] Facultad de Ciencias, Universidad Autónoma del Estado de Morelos, Ave. Universidad 1001, CP 62209, Cuernavaca, Morelos, México
[c] Cumhuriyet University, Physics Department, 58140 Sivas, Turkey
[d] Dokuz Eylül University, Physics Department, 35160 Buca, İzmir, Turkey

ARTICLE INFO

Article history:
Received 23 February 2013
Received in revised form
20 April 2013
Accepted 26 April 2013
Available online 7 May 2013

Keywords:
Nonlinear optics
Donor impurity
Quantum-well wires

ABSTRACT

The 1s-like and 2p-like donor impurity energy states are studied in a semiconductor quantum wire of equilateral triangular cross section as functions of the impurity position and the geometrical size of the structure. Linear and nonlinear coefficients for the optical absorption and relative refractive index change associated with 1s→2p transitions are calculated for both the *x*-polarization and *y*-polarization of the incident light. The results show a mixed effect of redshift and blueshift depending on the location of the donor atom. Also, strong nonlinear contributions to the optical absorption coefficient are obtained for both polarizations in the on-center impurity case.

1. Introduction

The study of semiconducting low-dimensional heterostructures has been a revolutionary fact in the physics of solid state that has allowed for undoubted milestones in the technology of electronic and optoelectronics devices. Many researches has been carried out in this context. So, to obtain a brief account of them we can, for instance, refer to the book by Harrison (and the number of references therein) [1].

In the particular subject of semiconductor quantum-well wires (QWWs) it is possible to mention—as a matter of examples—a rather early review on the optical properties [2], as well as a selection of articles published within the last 15 years [3–25]. Among the earlier works in this group we find several experimental studies on the optical properties of V-groove QWWs [3,4] and the nonlinear optics in CdSe and GaAs QWWs [5]; as well as the report on room temperature lasing [6], and on photoluminescence [9] of V-groove QWWs. The low-temperature electron mobility in V-shaped QWWs was calculated by Tsetseri et al. [10]. There are also works regarding exciton states, magnetoexcitons and exciton-related optical properties [13,19,21,22]; and even a report on electron g-factor in QWWs in the presence of spin-orbit Rashba coupling and magnetic field [23].

The knowledge of the properties of electrical and optical phenomena associated with shallow-donor impurities is of topmost importance in bulk semiconductors and in semiconducting low-dimensional systems. In this sense, the investigation of impurity-related effects in QWWs can show a number of publications [8,11,12,14–17]. These reports deal with different physical features such as the influence of the QWW cross section geometry, application of electric and magnetic fields, dielectric constant mismatch, position-dependence of the effective mass, hydrostatic pressure and temperature effects, and diamagnetic susceptibility.

The nonlinear optical properties [26] of low-dimensional semiconductor heterostructures have been a subject of great interest in past years [27]. Energy transitions between confined states in these artificial semiconducting systems usually associate with significant values of the oscillator strength [28] as well as small relaxation times [29]. In these structures, the rather large values of the oscillator strength are responsible for the appearance of high dipole moment expectation values. Therefore, it is possible to foresee pretty high manifestations of the nonlinear optical properties. Taking into account the rather extensive literature on the subject, we may refer, for instance, to the experimental observation of second harmonic generation (SHG) [30,31], the third harmonic generation (THG) [32] and the four wave mixing [33]. These reports have motivated the realization of many theoretical studies regarding the nonlinear optical rectification (NOR), THG and other optical nonlinearities in semiconductor heterostructures, among which we may cite the references [34–48]. In

(*) Corresponding author. Tel.: +57 4 219 56 30.
E-mail addresses: cduque@fisica.udea.edu.co, cduque_echeverri@yahoo.es (C.A. Duque).

0022-2313/$ - see front matter © 2013 Elsevier B.V. All rights reserved.
http://dx.doi.org/10.1016/j.jlumin.2013.04.048

quasi-one-dimensional structures, there are—for instance—reports on the influence of the electron–hole interaction on the electro-optical properties of hyperbolic QWWs [7], the hydrostatic pressure effect on the intersubband optical absorption and refractive index change in V-groove QWWs [18]; the optical absorption in asymmetric graded ridge QWWs [20], and the nonlinear optical absorption associated with shallow-hydrogenic impurities in GaAs/AlGaAs QWWs under hydrostatic pressure [24]. There is also a recent work of the nonlinear optical absorption in a QWW under magnetic field and Rashba spin-orbit effect [25].

Very recently, Khordad et al. have published a number of research articles dealing with semiconducting QWWs of triangular—and parallelogram-shaped—cross section [49–51]. The exact eigenfunctions of a QWW with equilateral triangular cross section were presented in Ref. [49] and used to obtain the nonlinear optical absorption response and the relative change in the refractive index in a GaAs-based structure. The generation of second and third harmonics in the same class of systems are the subject of study in Ref. [51].

With all this as a motivation, the aim of the present work is to present the results of the calculation of the linear and nonlinear optical absorption and relative change of the refractive index coefficients associated with the transitions $1s\rightleftarrows 2p_x$ and $1s\rightleftarrows 2p_y$, between shallow donor impurity states in a QWW of triangular cross-section. The organization of the work is as follows: Section 2 briefly presents the description of the theoretical model. In Section 3 one finds the corresponding results and discussion. Finally, Section 4 contains the main conclusions of the study.

2. Theoretical framework

The wire's cross section has a triangular shape with equal sides of length L. In our theoretical approach, we use the effective mass and parabolic approximations to describe the conduction band states in the heterostructure. Given the particular geometry of the system, the Cartesian coordinates are the suitable choice for writing the three-dimensional Hamiltonian

$$H=-\frac{\hbar^2}{2\,m^{(*)}}\left[\frac{\partial^2}{\partial x^2}+\frac{\partial^2}{\partial y^2}+\frac{\partial^2}{\partial z^2}\right]+V(x,y)-\frac{e^2}{\epsilon_r r}, \tag{1}$$

where $r=\sqrt{(x-x_i)^2+(y-y_i)^2+z^2}$ is the electron-impurity distance [(x,y,z) and $(x_i,y_i,0)$ correspond, respectively, to the electron and the impurity positions], $m^{(*)}$ ($=0.0665\,m_0$, where m_0 is the free electron mass) is the electron effective mass, ϵ_r ($=12.35$) is the GaAs static dielectric constant, e is the absolute value of the electron charge, and the confining 2D potential in the triangular region is

$$V(x,y)=\begin{cases}0, & \text{if } (x,y) \text{ is inside the wire region;}\\ \infty, & \text{if } (x,y) \text{ is outside the wire region.}\end{cases} \tag{2}$$

Without the impurity potential term at the right-hand side in Eq. (1), the motion along the z coordinate (wire's axis) is free and extends to infinity in both directions with wavefunction $\phi(z)\sim\exp(ik_z z)$, and free-particle-like energy $\varepsilon(k_z)=\hbar^2k_z^2/2\,m^{(*)}$. Under such specific conditions, the solution of the two-dimensional effective mass equation for the confined motion of the electron in the cross section of the triangular QWW, with infinite barriers (according to the Eq. (2))

$$-\frac{\hbar^2}{2\,m^{(*)}}\left[\frac{\partial^2}{\partial x^2}+\frac{\partial^2}{\partial y^2}\right]\psi(x,y)+V(x,y)\psi(x,y)=E_{2D}\psi(x,y), \tag{3}$$

was obtained by Khordad et al. with the help of group theory [49,51]. The allowed energies are given by

$$E_{2D}=E_{p,q}=(p^2+p\,q+q^2)\frac{8\,\pi^2\,\hbar^2}{3\,m^{(*)}L^2}, \tag{4}$$

whilst the corresponding unnormalized wavefunctions are

$$\psi_{p,q}(x,y)\sim\cos\left[\frac{2\pi xq}{L}\right]\sin\left[\frac{(2p+q)2\pi y}{\sqrt{3}L}\right]-\cos\left[\frac{2\pi xp}{L}\right]\sin\left[\frac{(2q+p)2\pi y}{\sqrt{3}L}\right]-\cos\left[\frac{2\pi x(p+q)}{L}\right]\sin\left[\frac{(p-q)2\pi y}{\sqrt{3}L}\right], \tag{5}$$

where $q=0,1,2,3,\ldots$, and $p=q+1,q+2,q+3,\ldots$.

The impurity states can be calculated by means of a variational procedure. We are interested in obtaining the 1s, $2p_x$, $2p_y$, and $2p_z$ impurity states associated with the electron ground state in the quantum wire ($q=0$, $p=1$, and $k_z=0$). In consequence, the trial wavefunctions are written as

$$\Psi_i(x,y,z)=N_i\psi_{1,0}(x,y)\Theta_i(r)\exp(-\lambda_i\,r), \tag{6}$$

where N_i is the normalization constant, λ_i is the variational parameter for the state under consideration, and $\Theta_i(r)=1,(x-x_i),(y-y_i)$, and z for the states 1s, $2p_x$, $2p_y$, and $2p_z$, respectively.

The energy of each donor impurity state associated with the Hamiltonian in Eq. (1), and the corresponding wavefunction, is obtained by minimizing the equation

$$\mathcal{E}(\lambda_i)=\frac{\langle\Psi_i(x,y,z)|H|\Psi_i(x,y,z)\rangle}{\langle\Psi_i(x,y,z)|\Psi_i(x,y,z)\rangle}, \tag{7}$$

with respect to the variational parameter. After the energy is obtained in Eq. (7), the donor impurity binding energy (E_b) is obtained from the usual definition

$$E_b=E_{1,0}-\mathcal{E}(\lambda_i^0) \tag{8}$$

where λ_i^0 is the value of λ_i which minimize the energy in Eq. (7).

With these states, and for x-polarization (y-polarization) of the incident radiation, we are then able to evaluate the transition matrix element $M_{fi}=\langle\Psi_f|x-L/2|\Psi_i\rangle$ ($=\langle\Psi_f|y-L\sqrt{3}/6|\Psi_i\rangle$), which will be in the core of the evaluation of the coefficients of optical absorption and of the relative change in the refractive index. The expressions for these quantities can be obtained within different contexts. One of the most commonly used is the compact density-matrix theory for the electronic polarization as a response to an electromagnetic field of frequency ω, [36,52,53]. They are

$$\alpha^{(1)}(\omega)=\omega\sqrt{\frac{\mu}{\epsilon_r}}\,\frac{e^2\,\sigma_v\,\hbar\,\Gamma_{if}\,|M_{fi}|^2}{(E_{fi}-\hbar\,\omega)^2+(\hbar\,\Gamma_{if})^2}, \tag{9}$$

$$\alpha^{(3)}(\omega,I)=-\omega\sqrt{\frac{\mu}{\epsilon_r}}\,\frac{I}{2\,\epsilon_0\,n_r\,c}\,\frac{e^4\sigma_v\,\hbar\,\Gamma_{if}\,|M_{fi}|^2}{[(E_{fi}-\hbar\,\omega)^2+(\hbar\,\Gamma_{if})^2]^2}\times\left\{4\left|M_{fi}\right|^2-\frac{|M_{ff}-M_{ii}|^2\,[3\,E_{fi}^2-4\,E_{fi}\,\hbar\,\omega+\hbar^2(\omega^2-\Gamma_{if}^2)]}{E_{fi}^2+(\hbar\Gamma_{if})^2}\right\}, \tag{10}$$

the linear and nonlinear optical absorption coefficients. In these expressions $E_{fi}=E_f-E_i$ is the transition energy difference, μ is the magnetic permeability of vacuum, ϵ_0 is the free-space dielectric permittivity, and c is the speed of light in vacuum. The Γ_{if} ($=5$ THz) are the damping rates associated to the transition, σ_v ($=3.8\times10^{22}$ m^{-3}) is the carrier density, and $n_r=\sqrt{\epsilon_r}$ is the GaAs refractive index. The quantity

$$I=2\sqrt{\frac{\epsilon_r}{\mu}}\left|E(\omega)\right|^2=\frac{2\,n_r}{\mu\,c}\,|E(\omega)|^2 \tag{11}$$

is the optical intensity of the incident wave. The total absorption coefficient is then given by the sum of the linear and nonlinear

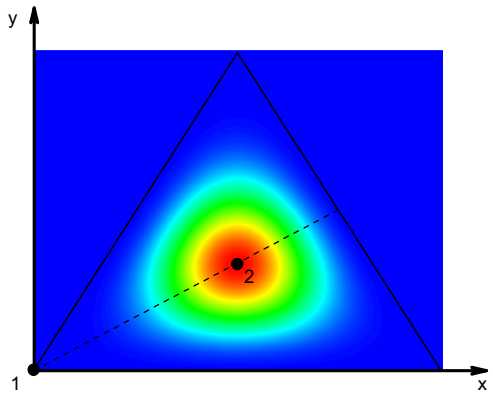

Fig. 1. Transversal section of the quantum-well wire. The color map corresponds to the amplitude of probability for the first confined non correlated electron state. The points 1 and 2 denote, respectively, the positions of on-corner and on-center impurities. The dashed line corresponds to the equation $y = x/\sqrt{3}$ along which the impurity moves in the present work. (For interpretation of the references to color in this figure caption, the reader is referred to the web version of this article.)

terms

$$\alpha(\omega, I) = \alpha^{(1)}(\omega) + \alpha^{(3)}(\omega, I). \tag{12}$$

Likewise, we have for the linear and nonlinear contributions to the relative change of the refractive index:

$$\frac{\Delta^{(1)}(\omega)}{n_r} = \frac{e^2\,\sigma_v\,|M_{fi}|^2}{2\,n_r^2\,\epsilon_0}\frac{E_{fi}-\hbar\,\omega}{(E_{fi}-\hbar\,\omega)^2+(\hbar\,\Gamma_{if})^2}, \tag{13}$$

$$\frac{\Delta^{(3)}(\omega, I)}{n_r} = -\frac{e^4\,\sigma_v\,\mu\,c\,I\,|M_{fi}|^2}{4\,n_r^2\,\epsilon_0}\frac{E_{fi}-\hbar\,\omega}{[(E_{fi}-\hbar\,\omega)^2+(\hbar\,\Gamma_{if})^2]^2} \times\left\{4\left|M_{fi}\right|^2-\frac{(M_{ff}-M_{ii})^2}{E_{fi}^2+(\hbar\,\Gamma_{if})^2}\left[E_{fi}(E_{fi}-\hbar\,\omega)-(\hbar\,\Gamma_{if})^2 -\frac{(\hbar\,\Gamma_{if})^2(2\,E_{fi}-\hbar\omega)}{E_{fi}-\hbar\omega}\right]\right\}. \tag{14}$$

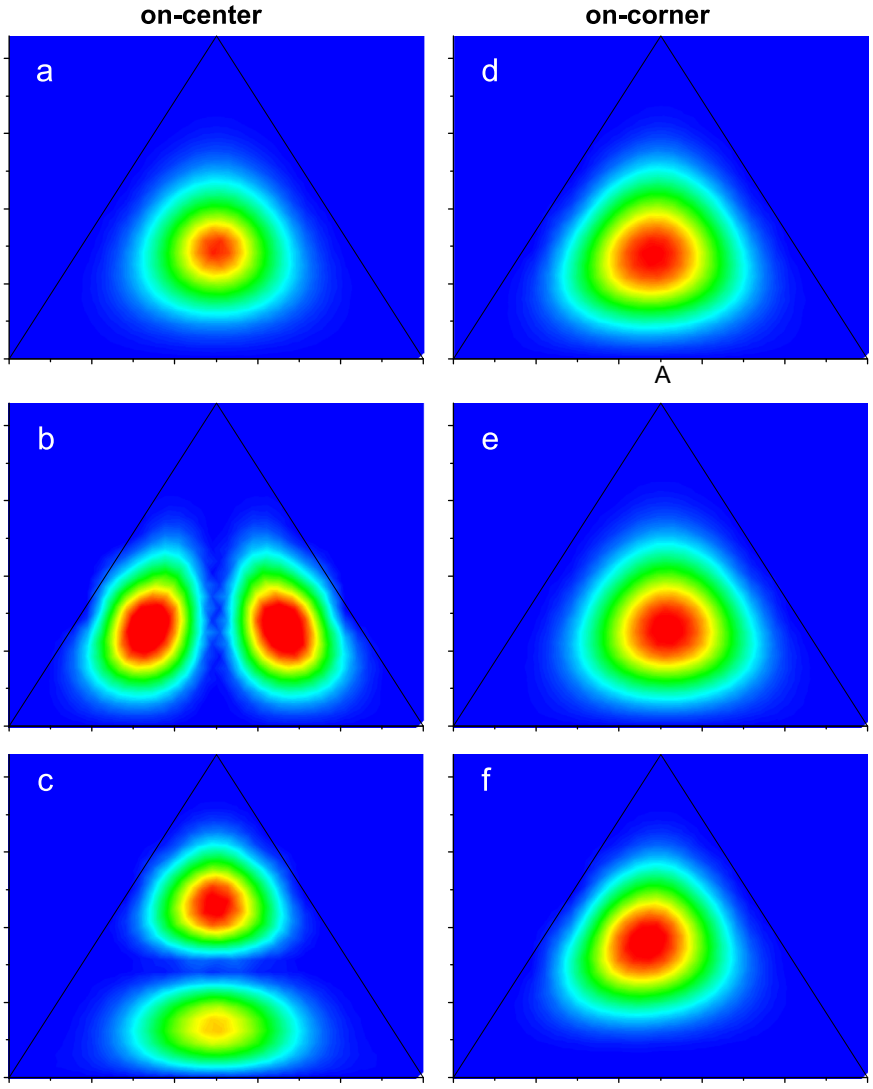

Fig. 2. The color map corresponds to the amplitude of probability for the first three hydrogenic impurity state (1s, $2p_x$, and $2p_y$). Left panel is for on-center impurities whereas the right-hand panel contains the results for on-corner impurities. In both cases, calculations are for $L = 10$ nm. (a) 1s, (b) $2p_x$, (c) $2p_y$, (d) 1s, (e) $2p_x$ and (f) $2p_y$. (For interpretation of the references to color in this figure caption, the reader is referred to the web version of this article.)

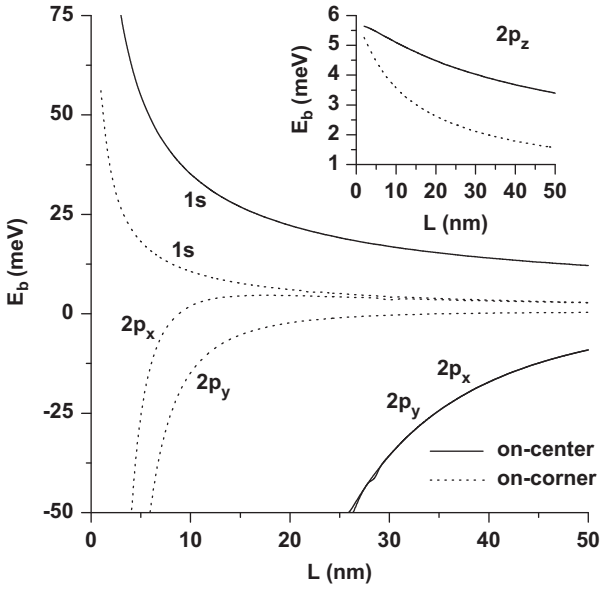

Fig. 3. Binding energy of the 1s-like and 2p-like hydrogenic donor impurity states in a triangular-shaped GaAs quantum-well wire as a function of the side of the triangle (L). The results are for on-center ($x_i = L/2$, $y_i = L\sqrt{3}/6$) and on-corner ($x_i = 0$, $y_i = 0$) impurities. The inset shows the binding energy for the $2p_z$-like state.

Analogously, the total relative change of the refractive index is the sum of these two contributions:

$$\frac{\Delta(\omega, I)}{n_r} = \frac{\Delta^{(1)}(\omega)}{n_r} + \frac{\Delta^{(3)}(\omega, I)}{n_r}. \tag{15}$$

On the other hand, taking advantage of the symmetry of the system, the position of the hydrogenic impurity atom is set to move along one of the triangle's medians, namely $\vec{r}_i = (x_i, x_i/\sqrt{3}, 0)$.

3. Results and discussion

The numerical outcome of the study is reported for the case of a GaAs-based QWW, as a prototypical system (see Fig. 1 for an illustrative scheme).

Fig. 2 shows a density plot for the probability of the impurity states associated with the $(q = 0,\ p = 1)$ uncorrelated ground electron level. Fig. 2(a)–(c) corresponds to the situation in which the impurity atom is placed at the triangle's orthocenter $(x = L/2,\ y = L/2\sqrt{3})$, whereas Fig. 2(d)–(f) represent the quantity $|\Psi_i(x, y, z)|^2$ in the case of the impurity located at the bottom left vertex of the triangle $(x = y = 0)$.

In Fig. 3 we are presenting the calculated 1s-like and 2p-like impurity binding energies related with the confined ground

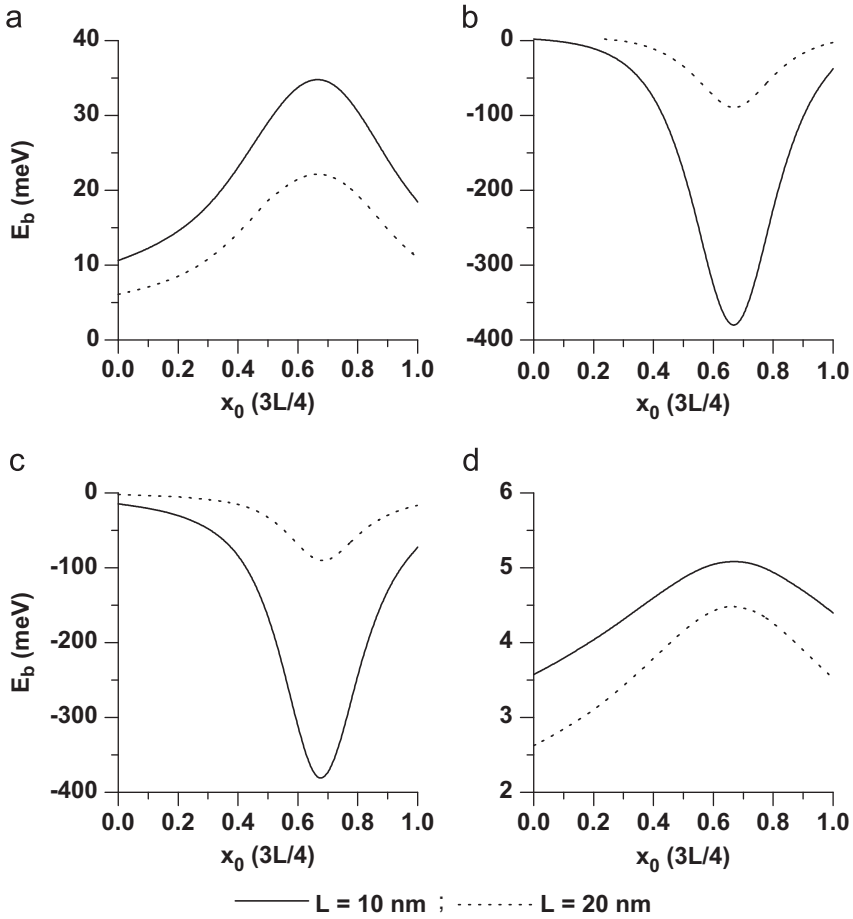

Fig. 4. Binding energy of the 1s-like and 2p-like hydrogenic donor impurity states in a triangular-shaped GaAs quantum-well wire as a function of the impurity position — the impurity moves along the line $y_i = x_i/\sqrt{3}$. The results are for $L = 10$ nm (solid lines) and $L = 20$ nm (dotted lines). (a) 1s, (b) $2p_x$, (c) $2p_y$ and (d) $2p_z$.

electron state in the wire. They are given as functions of the triangle side length for the two particular choices of the hydrogenic impurity position mentioned above. One may see that the limits that correspond to the strict one-dimensional (very small L) —consistent with the choice of the trial wavefunction—and three-dimensional effective hydrogen atom (large L) are appropriately approached in all cases. In the case of the 1s-like state, the convergence towards the limiting case of very large L in the on-center case is much slower than the one obtained for the on-corner impurity. This is mostly due to the stronger on-center Coulombic coupling provided that the electronic density of probability has its maximum located precisely at the impurity position. Although the 1s-like state keeps its central symmetry in the on-corner case, the magnitude of the Coulombic contribution (see Fig. 2(d)) is considerably smaller due to the effective spatial separation between the electron and the impurity core. In all, augmenting the size of the triangular cross section implies the reduction in the localization and, thus, in the strength of the Coulombic coupling; but the probability density still has its maximum around the orthocenter and, therefore the binding energy is larger when the impurity locates at the center.

An analogous discussion can be made in the case of the $2p_{x,y}$ binding energies. Given the central symmetry of the ground electron density of probability, the electrostatic interaction with the 2p orbitals is stronger in the on-center impurity configuration, thus leading to larger—in magnitude—values of E_b. This can be seen by observing the associated solid curve in Fig. 3. The negative sign is due to the usual choice for the energy reference in the description of the impurity binding energies (see Eq. (8)). Besides, the magnitude of the impurity binding energy is less affected by the increment in the triangle side length due to the lobular geometry of the density of probability of p orbitals. On the other hand, given that the triangular cross section is equilateral, both p_x and p_y symmetries are equivalent. Therefore, the corresponding binding energies are degenerate.

Analyzing the results shown for the on-corner impurity, we base on the plots appearing in Fig. 2(e) and (f). The positioning of the impurity atom at the $(0,0)$ vertex always leaves only one of the lobular parts of the p-like orbital with a significant overlapping with the uncorrelated ground electron state density of probability (see Fig. 1). This means that the effective electron-impurity distance is—in fact—larger, and the electrostatic interaction weakens. In order to explain the difference in magnitude of the $2p_x$ and $2p_y$ binding energies, we observe the density of probability depicted in Fig. 2(f). There, we notice a deviation of the electron cloud towards the left bottom vertex (the upper lobulus of the $2p_y$ orbital is pushed away by the lateral infinite barrier, towards the inner of the triangle). As a consequence, the value of the effective electron-impurity distance is smaller.

Regarding the $2p_z$ binding energy shown in the inset; its smallness can be directly justified by the extended character of the uncorrelated free-like electron wavefunction along the wire axial direction. This causes a large reduction in the Coulombic interaction due to the enlargement of the expected electron-impurity distance.

Fig. 4 contains the dependence of E_b upon the position of the donor impurity atom (along the $y = x/\sqrt{3}$ direction) for the 1s and 2p states under consideration. The configurations included are those of $L = 10$ nm and $L = 20$ nm. One readily sees that the maximum values, in all cases, correspond to the on-center situation. Furthermore, the results depicted confirm the decreasing behavior of E_b with respect to the increment in the triangle side length L, according the discussion made above.

On the other hand, Figs. 5 and 6 show, respectively, the variations of the $E_f - E_i$ electron transition energy as functions of the triangle size L and the impurity position. It is worth mentioning that this difference corresponds to the total energies of the electrons in the initial (1s) and final (2p) states involved in the transition.

It is obvious that the transition energies are rather strongly decreasing functions of the triangle size. This behavior relates with the loss in confinement of the electron motion which reflects in the reduction of the Coulombic interaction curves (see the respective changes in the energy positions of the solid and dotted curves in Fig. 3 while L augments) and of the uncorrelated energy $E_{1,0}$, according to the Eq. (4).

Regardless the size of the triangular cross section, the maximum value of the transition energy is the one obtained when the donor impurity atom is at the center. This is consistent with the results previously commented.

In Figs. 7 and 8 we are presenting the different dipole moment matrix elements that are included in our study of the optical properties. They contain the functional variations of these elements with respect to L and the donor impurity position, respectively.

Fig. 7 shows the dipole matrix elements, taking into account two particular polarizations of the light; x-polarization (Fig. 7 (a) and (c)), and y-polarization (Fig. 7(b) and (d)), as well as the two specific positions of the impurity already discussed (on-center: Fig. 7(a) and (b); and on-corner: 7(c) and (d)).

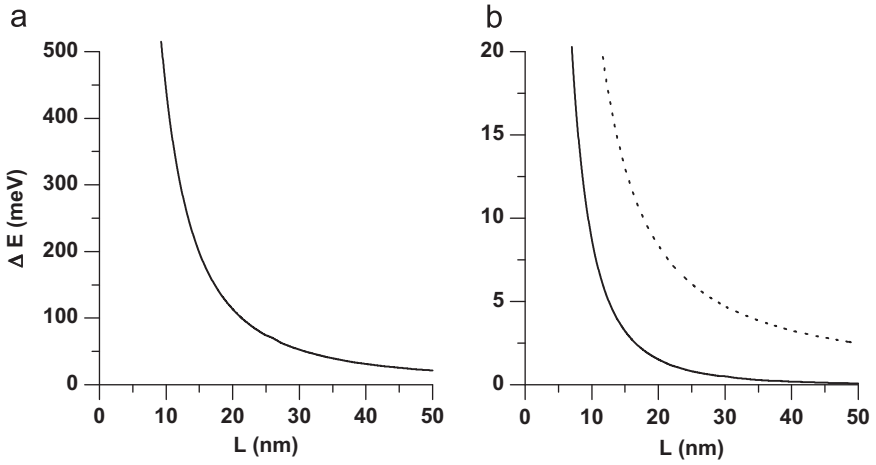

Fig. 5. Energy transition between the first confined hydrogenic donor impurity states in a triangular-shaped GaAs quantum-well wire as a function of the side of the triangle. The solid lines are for $1s \rightarrow 2p_x$ transitions whereas the dotted lines are for $1s \rightarrow 2p_y$ transitions. Two different impurity positions have been considered: on-center impurity (a) and on-corner impurity (b). Note the superposition of both energy transitions in (a).

The growing variation exhibited by the line 1 (dipole matrix element $M^2_{1s-2p_x}$ of x–x_i, in the on-center case) in Fig. 7 (a) associates with the finite result of the integral along the x-direction given the even parity of the integrand. We must keep in mind that along the y-direction, both 1s and $2p_x$ lose their symmetries due to the presence of an upper barrier formed by the intersection of two planes, as well as a lower horizontal barrier related with a single plane. The other matrix elements, evaluated under the x-polarization, identically vanish for symmetry reasons. The opposite situation appears in the evaluation of the dipole matrix elements in the on-center case under the y-polarization. This time, M_{1s-2p_x} is zero because the integration over the variable

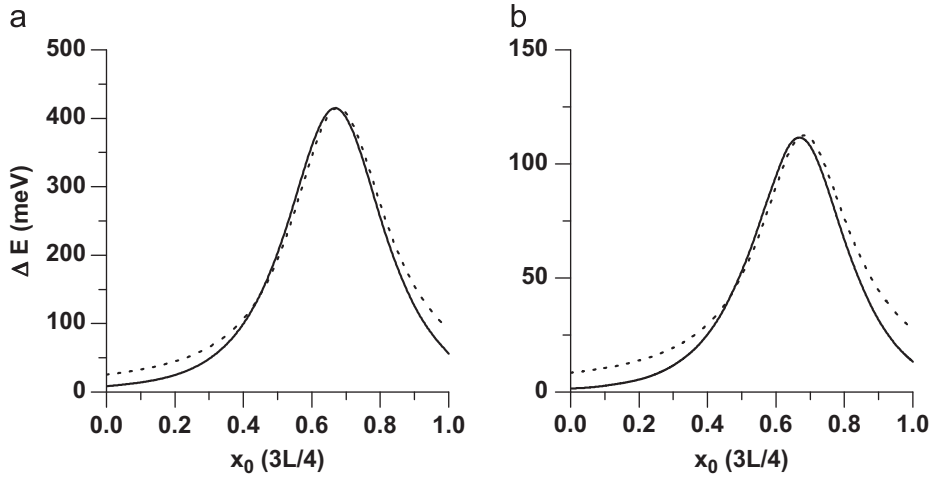

Fig. 6. Energy transition between the first confined hydrogenic donor impurity states in a triangular-shaped GaAs quantum-well wire as a function of the impurity position —the impurity moves along the line $y_i = x_i/\sqrt{3}$. The solid lines are for $1s \rightarrow 2p_x$ transitions whereas the dotted lines are for $1s \rightarrow 2p_y$ transitions. Two different values of the lateral side of the wire have been considered: 10 nm (a) and 20 nm (b).

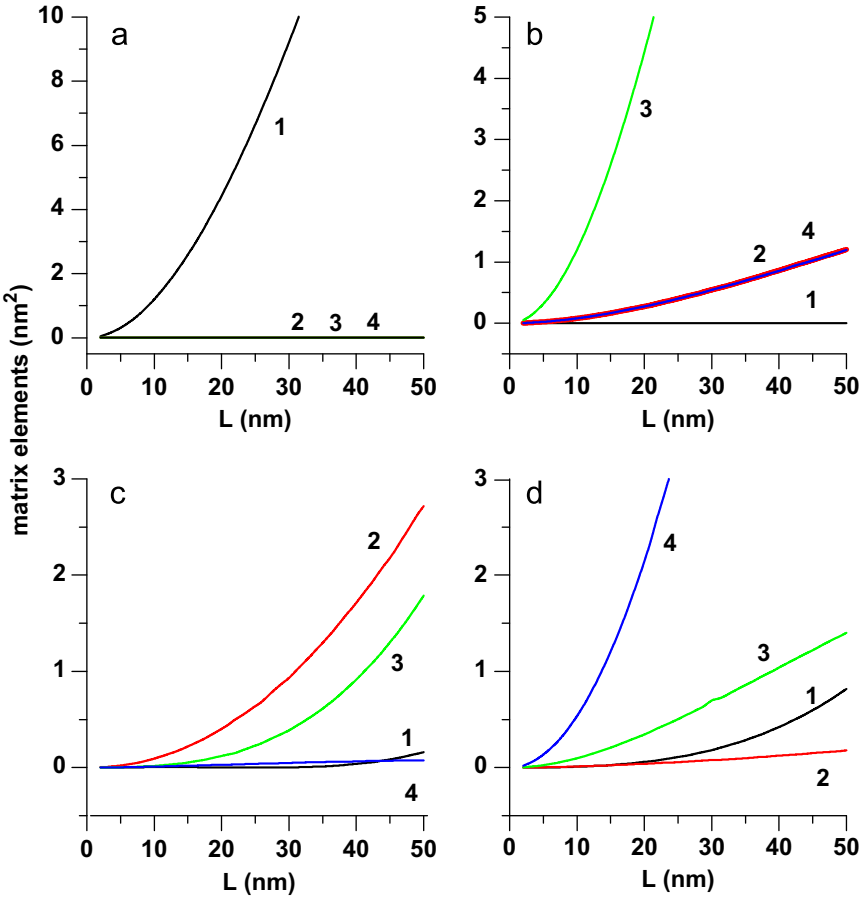

Fig. 7. Matrix elements for the transition between the first confined hydrogenic donor impurity states in a triangular-shaped GaAs quantum-well wire as a function of the side of the triangle (L). The results are as follows: on-center impurity (a, b), on-corner impurity (c, d), x-polarization (a, c), y-polarization (b, d). The numbers and colors identify the following matrix elements: $M^2_{1s-2p_x}$ (1-black), $(M_{1s-1s}-M_{2p_x-2p_x})^2$ (2-red), $M^2_{1s-2p_y}$ (3-green), and $(M_{1s-1s}-M_{2p_y-2p_y})^2$ (4-blue). (For interpretation of the references to color in this figure caption, the reader is referred to the web version of this article.)

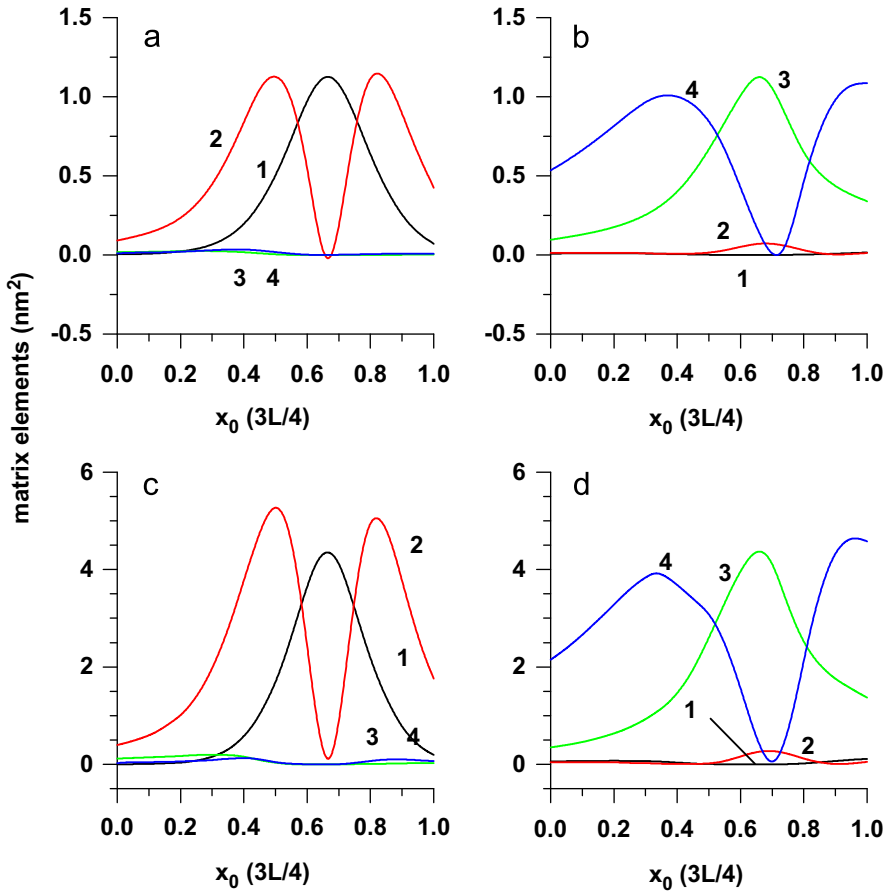

Fig. 8. Matrix elements for the transition between the first confined hydrogenic donor impurity states in a triangular-shaped GaAs quantum-well wire as a function of the impurity position —the impurity moves along the line $y_i = x_i/\sqrt{3}$. The results are as follows: $L=10$ nm (a, b), $L=20$ nm (c, d), x-polarization (a, c), y-polarization (b, d). The numbers and colors identify the following matrix elements: $M^2_{1s-2p_x}$ (1-black), $(M_{1s-1s}-M_{2p_x-2p_x})^2$ (2-red), $M^2_{1s-2p_y}$ (3-green), and $(M_{1s-1s}-M_{2p_y-2p_y})^2$ (4-blue). (For interpretation of the references to color in this figure caption, the reader is referred to the web version of this article.)

x has an odd integrand. The remaining dipole matrix elements are finite, with a predominance of the term M_{1s-1s} (that is why we observe a coincidence of lines 2 and 4). The behavior of the element M_{1s-2p_y}, represented by the line 3, is analogous to the one shown by the line 1 in Fig. 7(a). That is, there is no spatial symmetry involved in the integration along y, and the increase in L leads to larger values of $y-y_i$ in the integrand.

In the on-corner case, none of the wavefunctions show a definite symmetry. Therefore, all dipole matrix elements are non-zero, although in Fig. 7(c) and (d) it seems that some of the lines have null values; but it is merely for scale reasons. What happens in fact is that in the x-polarization (Fig. 7(c)), the dominant terms are M_{1s-2p_x} and $M_{2p_x-2p_x}$, whilst in the y-polarization (Fig. 7(d)) they are M_{1s-2p_y} and $M_{2p_y-2p_y}$.

Explaining the results of the functional variation of the same dipole matrix elements with respect to the change in the donor impurity position (Fig. 8(a)–(d)) implies the use of analogous arguments. One sees that, in general, the dipole matrix elements are nonzero (there are also scale reasons involved, depending on the specific polarization of the incident light), with the exception of those symmetry points previously discussed in the analysis of Fig. 7.

We shall discuss now the outcome of the calculation of the optical absorption response and the relative change of the refractive index associated to donor impurity states in the GaAs-based triangular QWW. Accordingly, the variations of $\alpha^{(1)}$, $\alpha^{(3)}$, and α are shown in Fig. 9(a) and (b) for x- and y-polarizations, respectively, in the on-center-impurity configuration, for three particular values of the triangle side length.

It is possible to see that for a fixed value of L there is only a very small difference in the amplitudes of the isolated contributions and the total absorption coefficient, when comparing the results of the two polarizations. Meanwhile, the peak positions are, as can be expected, the same in both cases. Thus, the numerical difference lies in the magnitude of the transition matrix elements. By observing Fig. 7(a) and (b) we notice that, for the y-polarization the element M_{1s-2p} is somewhat smaller than its corresponding one in the x-polarization. At the same time, the element of the type $|M_{1s-1s}-M_{2p-2p}|$ is slightly larger than that of the x-polarization case. Augmenting the side length, L, reflects in the redshift of the peak positions, Whilst the amplitude of the linear term resonant peak becomes practically unaffected because of the compensating competition between the growth in the transition dipole matrix element and the fall in the resonance frequency; the nonlinear term does exhibits rather important changes in amplitude as long as the size of the triangle increases. What is happening in this situation is that there is a predominance coming from the factor including the fourth power of the transition dipole matrix element, given the smallness of $|M_{1s-1s}-M_{2p-2p}|$ in each case.

We can also notice that the magnitude of the amplitude of the nonlinear resonant peak reaches a quite significant weight for the value of light intensity chosen ($I = 0.95 \times 10^{10}$ W/m^2). In consequence, there is an important quenching effect on the total

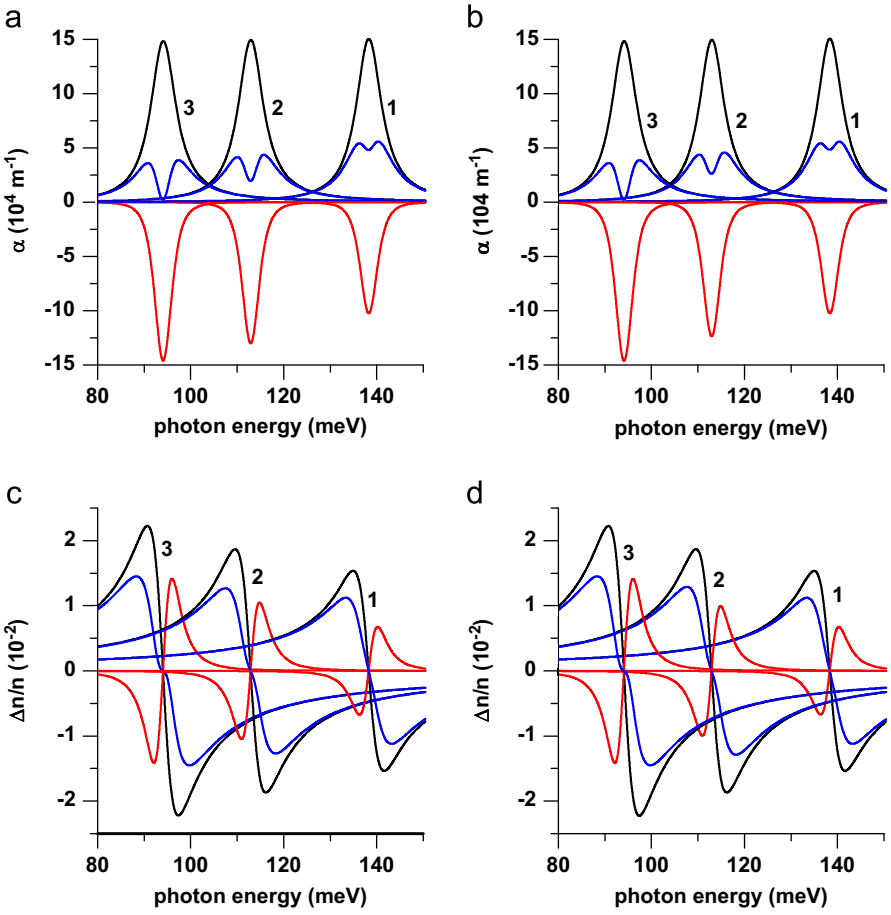

Fig. 9. Donor-impurity-related linear (black line), nonlinear (red line) and total (blue line) optical absorption coefficient (a, b) and relative change in the refractive index (c, d) as functions of the energy of the incident photon in a triangular-shaped GaAs quantum-well wire for on-center impurity configuration. The results are as follows: x-polarization for $1s$–$2p_x$ transitions (a, c), y-polarization for $1s$–$2p_y$ transitions (b, d). Three values of the side of the triangle have been considered: 18 nm (1), 20 nm (2), and 22 nm (3). (For interpretation of the references to color in this figure caption, the reader is referred to the web version of this article.)

absorption coefficient, even leading to the possibility of an absorption bleaching, as noticed in the case of $L=22$ nm in Fig. 9(a) and (b).

With regard to the relative change in the refractive index in this on-center impurity configuration [Fig. 9(c) and (d)], we are able to observe the same redshift as a result of the increase in the triangle size. The same explanation stated above applies in this case. The distinctive fact here is that the growth in L affects in the same way the amplitude of the linear and nonlinear contributions. So, the larger the triangle side is, the higher is the peak amplitude of $\Delta n/n_r$. The reason for this is the growing variation of the transition dipole matrix element as a function of L shown in Fig. 7(a) and (b) (see also Eqs. (12) and (14)).

Let us consider now the results for the optical absorption and relative refractive index change coefficients shown in Fig. 10. They correspond to the change in the donor impurity position along the line $y=x/\sqrt{3}$ (with the origin placed at the lower bottom vertex, as illustrated in Fig. 1) when the triangle size is kept fixed at $L=10$ nm.

In the case of the x-polarization [$1s$–$2p_x$ transition, Fig. 10 (a) and (c)], the increment in the horizontal position of the donor impurity has a mixed effect on the resonant peak position. First, there is a blueshift and, when the donor atom goes beyond the middle of the side length, the peak position becomes redshifted. Likewise, the peak amplitude of the linear and nonlinear contributions has first an increase and, when the impurity position goes beyond the center, this quantity diminishes. We can analyze such a behavior with the combined help of Figs. 6(a) and 8(a), for the transition energy and dipole moment matrix elements, respectively. With those results in mind, the optical properties under consideration are readily explained.

For the y-polarization [$1s$–$2p_y$ transition, Fig. 10(b) and (d)], increasing the value of the horizontal impurity position results in the same combined displacement (first a blueshift and then a redshift) although the subsequent shift towards the red is less pronounced. Also, the peak amplitudes start augmenting and bear an ulterior decrease when $x_i > L/2$. Again, Figs. 6(b) and 8 (b) contain the elements to explain the variation of these two optical responses.

4. Conclusions

In this paper we have studied the donor impurity states and the associated linear and nonlinear optical absorption and relative refractive index change coefficients in a triangular-shape GaAs quantum wire.

The calculation of the impurity binding energy considers 1s, $2p_x$, $2p_y$, and $2p_z$ states, coupled to the ground uncorrelated electron level in the system. The inclusion of a change in the position of the donor atom shows that the magnitude of the binding energy is larger when it coincides with the triangle's orthocenter. Likewise, the energies that correspond to the $1s$–$2p_{x,y}$ transitions and the corresponding dipole matrix elements have their maxima in the on-center case.

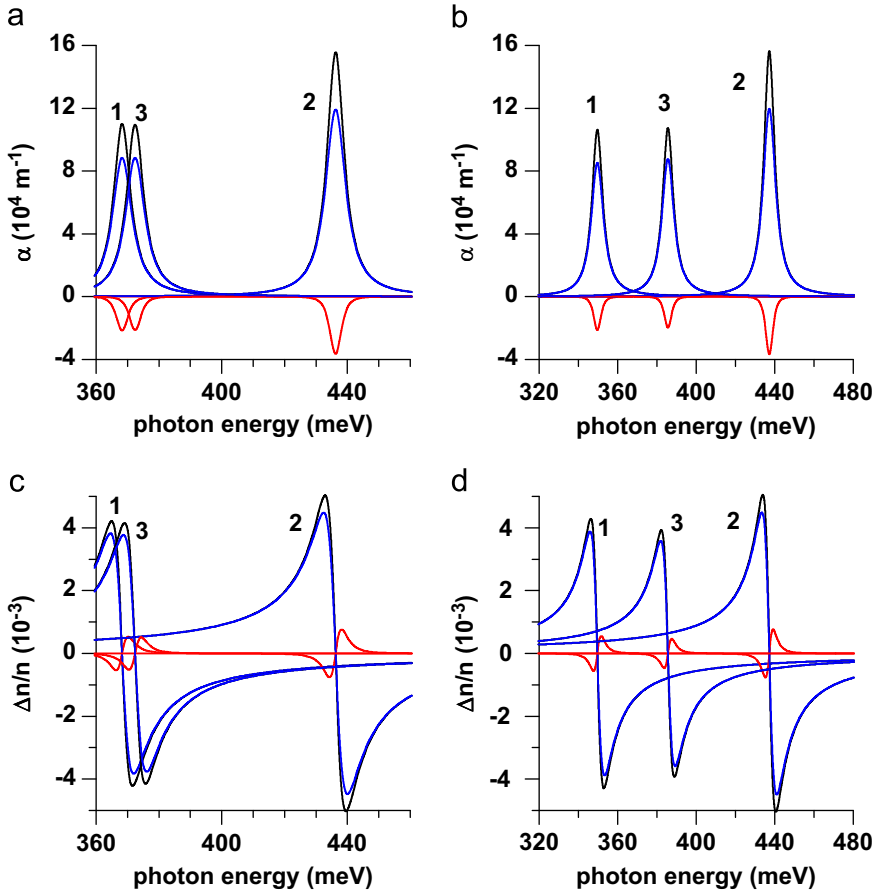

Fig. 10. Optical absorption (a, b) and changes in the refractive index (c, d) as a function of the energy of the incident photon in a triangular-shaped GaAs quantum-well wire with $L=10$ nm. The results are as follows: x-polarization for $1s$–$2p_x$ transitions (a, c), y-polarization for $1s$–$2p_y$ transitions (b, d). Three values of the impurity position have been considered: 4.5 nm (1), 5.0 nm (2), and 5.5 nm (3). (For interpretation of the references to color in this figure caption, the reader is referred to the web version of this article.)

With the calculated transition energies and impurity-related states we evaluated the linear and third-order nonlinear contributions to the optical absorption coefficient obtaining an overall redshift for the on-center case, when the side dimension of the triangular cross section is augmented, in both the x- and y-polarizations. An interesting fact is that the magnitude of the nonlinear term of the optical absorption can reach significant values, with the possibility of an absorption bleaching in the system. This makes the impurity states in a triangular-shaped quantum wire to be good candidates for the practical obtention of nonlinear optical responses using GaAs.

Acknowledgments

MEMR thanks Mexican CONACYT for support through 2011–2012 sabbatical Grant no. 180636, and research Grant CB-2008-101777. He is also grateful to the Escuela de Ingeniería de Antioquia and the Universidad de Antioquia for hospitality during his sabbatical stay. CAD is grateful to the Colombian Agencies CODI-Universidad de Antioquia (Estrategia de Sostenibilidad 2013-2014 de la Universidad de Antioquia) and Facultad de Ciencias Exactas y Naturales-Universidad de Antioquia (CAD-exclusive dedication project 2012–2013). The authors are grateful to The Scientific and Technological Research Council of Turkey (TÜBİTAK) for a research Grant (TÜBİTAK 109T650). The work was developed with the help of CENAPADSP, Brazil.

References

[1] P. Harrison, Quantum Wells, Wires and Dots, second ed., Wiley, Chichester, 2005.
[2] K. Kash, J. Lumin. 46 (1990) 69.
[3] M.J. Steer, D.J. Mowbray, M.S. Skolnick, W.R. Tribe, A.N. Forshaw, D. M. Whittaker, J.S. Roberts, A.G. Cullis, G. Hill, M. Pate, C.R. Whitehouse, Physica E 2 (1998) 949.
[4] Y. Ducommun, E. Martinet, H. Weman, G. Biasol, A. Gustafsson, E. Kapon, Physics E 2 (1998) 954.
[5] V. Dneprovskii, E. Zhukov, Superlatt. Microstruct. 23 (1998) 1217.
[6] T.G. Kim, X.-L. Wang, R. Kaji, M. Ogura, Physica E 7 (2000) 508.
[7] K. Guo, C. Chen, T.P. Das, Physica E 15 (2002) 192.
[8] E. Kasapoglu, H. Sari, I. Sokmen, Physica E 19 (2003) 332.
[9] S. Huang, Z. Chen, L. Bai, F. Wan, X. Chen, Sci. China Ser. G 48 (2005) 361.
[10] M. Tsetseri, G.P. Triberis, M. Tsaousidou, Superlatt. Microstruct. 43 (2008) 340.
[11] V.N. Mughnetsyan, M.G. Barseghyan, A.A. Kirakosian, Superlatt. Microstruct. 44 (2008) 86.
[12] A. Bilekkaya, Ş. Aktaş, S.E. Okan, F.K. Boz, Superlatt. Microstruct. 44 (2008) 96.
[13] S. Elagoz, H.D. Karki, P. Başer, I. Sokmen, Superlatt. Microstruct. 45 (2009) 506.
[14] R. Khordad, Physica E 42 (2010) 1503.
[15] E. Kasapoglu, F. Ungan, H. Sari, I. Sokmen, Physica E 42 (2010) 1623.
[16] P. Villamil, Physica E 42 (2010) 2436.
[17] R. Khordad, Eur. Phys. J. B 78 (2010) 399.
[18] R. Khordad, S. Kheiryzadeh Khaneghah, M. Masoumi, Superlatt. Microstruct. 47 (2010) 538.
[19] N. Arunachalam, C. Yoo, A. John-Peter, Superlatt. Microstruct. 49 (2011) 43.
[20] E. Sadeghi, Superlatt. Microstruct. 49 (2011) 91.
[21] N. Arunachalam, A. John-Peter, C.K. Yoo, J. Lumin. 132 (2012) 1311.
[22] S.D. Wu, L. Wan, Eur. Phys. J. B 85 (2012) 12.
[23] A. Gharaati, R. Khordad, Superlatt. Microstruct. 51 (2012) 194.
[24] M. Santhi, A. John-Peter, C.K. Yoo, Superlatt. Microstruct. 52 (2012) 234.
[25] R. Khordad, J. Lumin. 13 (2013) 201.
[26] S. Kielich, Ferroelectrics 4 (1972) 257.
[27] S. Schmitt-Rink, D.S. Chemla, D.A.B. Miller, Adv. Phys. 38 (1989) 89.
[28] L.C. West, S.J. Eglash, Appl. Phys. Lett. 46 (1985) 1156.

[29] J. Baier, I.M. Bayanov, U. Plodereder, A. Seilmeier, Superlatt. Microstruct. 19 (1996) 9.
[30] A. Bitz, M. Marsi, E. Tuncel, S. Gürtler, J.L. Staehli, B.J. Vartanian, M.J. Shaw, A.F. G. van der Meer, Phys. Rev. B 26 (1997) 19428.
[31] A. D'Andrea, N. Tomassini, L. Ferrari, M. Righini, S. Sedlci, M.R. Bruni, D. Schumarini, M.G. Simeone, Phys. Status Solidi A 164 (1997) 383.
[32] C. Sirtori, F. Capasso, D.L. Sivco, A.Y. Cho, Phys. Rev. Lett. 68 (1992) 1010.
[33] D. Warlod, S.Y. Auyang, P.A. Wolff, M. Sugimoto, Appl. Phys. Lett. 59 (1991) 2932.
[34] I. Karabulut, M.E. Mora-Ramos, C.A. Duque, J. Lumin. 131 (2011) 1502.
[35] L. Tsang, S.-L. Chuang, S.M. Lee, Phys. Rev. B 41 (1990) 5942.
[36] E. Rosencher, Ph. Bois, Phys. Rev. B 44 (1991) 11315.
[37] C. Lien, Y. Huang, J. Wang, J. Appl. Phys. 76 (1994) 1008.
[38] Y. Huang, Ch. Lien, J. Appl. Phys. 75 (1994) 3223.
[39] E. Rosencher, A. Fiore, B. Vinter, V. Berger, Ph. Bois, J. Nagle, Science 271 (1996) 168.
[40] A. Liu, S.-L. Chuang, C.Z. Ning, Appl. Phys. Lett. 76 (2000) 333.
[41] I. Karabulut, U. Atav, H. Safak, M. Tomak, Eur. Phys. J. B 55 (2007) 283.
[42] M. Załuz`ny, Phys. Rev. B 47 (1993) 3995.
[43] R. Wei, W. Xie, Curr. Appl. Phys. 10 (2010) 757.
[44] I. Karabulut, H. Safak, M. Tomak, Solid State Commun. 135 (2005) 735.
[45] S. Baskoutas, E. Paspalakis, A.F. Terzis, J. Phys.: Condens. Matter 19 (2007) 395024.
[46] W. Xie, Physica B 404 (2009) 4142.
[47] G. Wang, Q. Guo, L. Wu, X. Yang, Physica E 39 (2007) 75.
[48] H. Yildirim, M. Tomak, Phys. Rev. B 72 (2005) 115340.
[49] R. Khordad, S. Tafaroji, R. Katebi, A. Ghanbari, Commun. Theor. Phys. 57 (2012) 1076.
[50] R. Khordad, J. Theor. Appl. Phys. 6 (2012) 19.
[51] R. Khordad, S. Tafaroji, Physica E 46 (2012) 84.
[52] D. Ahn, S.-L. Chuang, IEEE J. Quantum Electron. QE-23 (1987) 2196.
[53] T. Takagahara, Phys. Rev. B 36 (1987) 929.